Applied Clay Science 213 (2021) 106244

Contents lists available at ScienceDirect

Applied Clay Science

journal homepage: www.elsevier.com/locate/clay

Partial rehydration of tubular halloysite (7 Å) immersed in $La(NO_3)_3$ solution for 3 years and its implication for understanding REE occurrence in weathered crust elution-deposited rare earth ores

Junming Zhou [a,b], Mengyuan Li [a,b], Peng Yuan [a,*], Yun Li [c], Hongmei Liu [a], Wenxiao Fan [a,b], Dong Liu [a], Huan Zhang [a,b]

[a] CAS Key Laboratory of Mineralogy and Metallogeny/Guangdong Provincial Key Laboratory of Mineral Physics and Materials, Guangzhou Institute of Geochemistry, CAS Center for Excellence in Deep Earth Science, Chinese Academy of Sciences, Guangzhou 510640, China
[b] University of Chinese Academy of Sciences, Beijing 100049, China
[c] Academy for Advanced Interdisciplinary Studies, Southern University of Science and Technology, Shenzhen 518055, China

ARTICLE INFO

Keywords:
Halloysite
Kaolinite
Rehydration
Weathered crust elution-deposited rare earth ores
La(III) ions

ABSTRACT

Clay minerals are the main carriers of rare earth elements (REE) in weathered crust elution-deposited rare earth (WED-RE) ores. The clay mineral-water interface reaction is among the most important interactions controlling the aggregation and transportation of REE(III) ions. Yet long-term experiments of interactions between REE(III) ions and clay minerals are scarce in the literature. Here, two typical clay minerals that commonly occur in WED-RE ores, namely tubular halloysite (7 Å) and platy kaolinite, were immersed in a La solution for 3 consecutive years. The specimens' characteristics were systematically determined using X-ray diffraction (XRD), transmission electron microscope (TEM), infrared spectroscopy (IR), and X-ray photoelectron spectroscopy (XPS). The partial rehydration of tubular halloysite (7 Å) was observed, with the resulting rehydrated halloysite characterized by lattice fringes having $d_{(001)}$-values of ~1.000 and 0.830 nm, whose distribution features demonstrated that the partial rehydration happened initially at the outermost layers of the halloysite (7 Å). By contrast, both the morphology and structure of kaolinite remained intact after its 3-year-long immersion in the La solution. For both immersed halloysite and kaolinite, the La existed as inner-sphere complexes, outer-sphere complexes, and hydroxide particles adsorbed on the surface of minerals. However, La(III) ions partially penetrated the interlayer of halloysite but did not enter that of kaolinite. Accordingly, the intercalation of La(III) in halloysite may facilitate the rehydration of halloysite (7 Å). These experimental results provide novel insight into the conditions for rehydrating tubular halloysite (7 Å), and indicate a new possible state of REE(III) in WED-RE ores, both of which help us to better understand the geochemical behavior of REE and clay minerals in WED-RE ores.

1. Introduction

Weathered crust elution-deposited rare earth (WED-RE) ore, also called ion-adsorption clays (Kynicky et al., 2012) or regolith-hosted ion-adsorption deposits (Borst et al., 2020), is one type of the most important resources of rare earth elements (REE) around the world (Chakhmouradian and Wall, 2012). The WED-RE ores now provide over 20% of global REE consumption (Borst et al., 2020; Garcia et al., 2017; Li et al., 2019b). In WED-RE ores, clay minerals such as tubular halloysite and platy kaolinite are the primary hosts of REE (Sanematsu and Watanabe, 2016), which exist as exchangeable trivalent ions in the clay minerals (Borst et al., 2020).

The WED-RE ores are formed by the chemical weathering of various bedrocks (e.g., granite) (Bao and Zhao, 2008; Sanematsu and Watanabe, 2016) and are widely distributed in warm and moist regions, predominantly in southern China (Kynicky et al., 2012; Sanematsu and Watanabe, 2016; Xie et al., 2016), as well as parts of Thailand (Sanematsu et al., 2013), Laos (Sanematsu et al., 2011), Vietnam (Yaraghi et al., 2019), Malaysia (Yaraghi et al., 2020), Brazil (Vieira et al., 2019), and Madagascar (Ram et al., 2019). In these regions, rainfall is abundant (e.

* Corresponding author at: CAS Key Laboratory of Mineralogy and Metallogeny, Guangzhou Institute of Geochemistry, Chinese Academy of Sciences (CAS), Wushan, Guangzhou 510640, China.
E-mail address: yuanpeng@gig.ac.cn (P. Yuan).

https://doi.org/10.1016/j.clay.2021.106244
Received 4 July 2021; Received in revised form 5 August 2021; Accepted 9 August 2021
Available online 17 August 2021

g., annual rainfall >1500 mm in south China) (Li et al., 2017; Woo et al., 1997), leading to the intense chemical weathering of various rocks (Sanematsu and Watanabe, 2016; Viers et al., 2007), with the depth of the weathered profile reaching 60 m in some WED-RE ores (Sanematsu and Watanabe, 2016).

Water (e.g., rainwater) is a key ingredient for REE mineralization in WED-RE ores. Being a solvent that is often involved in rock erosion reactions (e.g., the alteration of silicates) (Viers et al., 2007), water greatly influences the weathering of the earth's surface by dissolving ions from rocks (Dodds and Whiles, 2020). This dissolution and alteration release trivalent REE(III) ions from various accessory minerals (e.g., bastnaesite, xenotime, and allanite) (Bao and Zhao, 2008) and transform the rock-forming minerals (e.g., feldspar and mica) into clay minerals (Galán and Ferrell, 2013; Lanson et al., 2002; Lu et al., 2016). In this way, the abovementioned process provides the sources of ore-forming materials (i.e., the exchangeable REE(III) ions) and their carriers (i.e., clay minerals) of this type of REE ore. Furthermore, water can influence the surface properties of clay minerals (Schoonheydt and Johnston, 2013) and is associated in weathered crusts with the geochemical behavior of exchangeable REE(III) ions, such as their migration, adsorption, and desorption (Li et al., 2020; Nesbitt, 1979; Schoonheydt and Johnston, 2013; Sanematsu and Watanabe, 2016) (Chi et al., 2012; Tian et al., 2010), all of which are the vital processes for REE enrichment.

A significant percentage of rainwater becomes groundwater (Saxton and Rawls, 2006; Zhang, 2011). This groundwater generally persists over several years in weathered crusts (Gleeson et al., 2016; Zhang, 2011) and is closely related to the migration and accumulation of REE in the WED-RE ores (Huang et al., 2021; Li et al., 2020). Moreover, clay minerals undergo a structural transformation when exposed to water over the long term, which may influence the transformation of ions in those weathered crusts. For example, Joussein et al. (2006) found that, under the combined action of cations and water for 3 months, the spheroidal halloysite (7 Å) formed halloysite (10 Å) with a higher cation exchange capacity (CEC) than halloysite (7 Å) (Joussein, 2016; Yaraghi et al., 2020). The occurrence of halloysite (10 Å) in WED-RE ores could lead to greater enrichment of REE ions (Ram et al., 2019). Nevertheless, in the WED-RE ores, halloysite with a tubular morphology is the dominant form present (Li and Zhou, 2020; Ram et al., 2019). In fact, this tubular halloysite together with platy kaolinite are the paramount carriers of exchangeable REE(III) in the WED-RE ores (Kynicky et al., 2012; Li and Zhou, 2020; Ram et al., 2019). Yet how water affects the structure of these clay minerals and the geochemical behavior of REE (III) over a long-time span is still unclear.

In this work, tubular halloysite (7 Å) and platy kaolinite were immersed by La(III) aqueous solution for 3 years. La(III) ions served as a model REE(III) ion because of their similar chemical properties to REE (III) ions (Bau, 1999; Henderson, 1984). The morphology and structure of immersed halloysite and kaolinite, and the chemical state of La on these samples were systematically characterized, by using X-ray diffraction (XRD), transmission electron microscope (TEM), infrared spectroscopy (IR), and X-ray photoelectron spectroscopy (XPS). Interestingly, the rehydration of tubular halloysite (7 Å) in La(III) solution was observed in our study. This rehydrated halloysite affected the immobilization of La(III) in turn. These results shed new light on the stability and structure of halloysite (7 Å) and enhance the understanding of the REE(III) geochemical behavior in weathered crusts as affected by clay minerals.

2. Materials and methods

2.1. Materials and the immersion experiment

Halloysite (Hal) was collected from Linfen, Shanxi Province, China, and was purified by handpicking it and via its repeated sedimentation (Du et al., 2018). This Hal material generally included both halloysite (7 Å) and halloysite (10 Å) (Du et al., 2018); to exclude the latter's occurrence, the material was heated in an oven at 60 °C and sieved a 200-mesh size. Kaolinite (Kaol) was collected from Maoming, Guangdong Province, China. Exactly 2.000 g of Hal or Kaol was homogeneously mixed into 2.000 L of La(III) aqueous solution, and then both suspensions were sealed under atmospheric pressure and placed in laboratory for 3 years without any agitation. The temperature is the same as the room temperature in Guangzhou, which ranges from ~11 °C to ~34 °C from winter to summer.

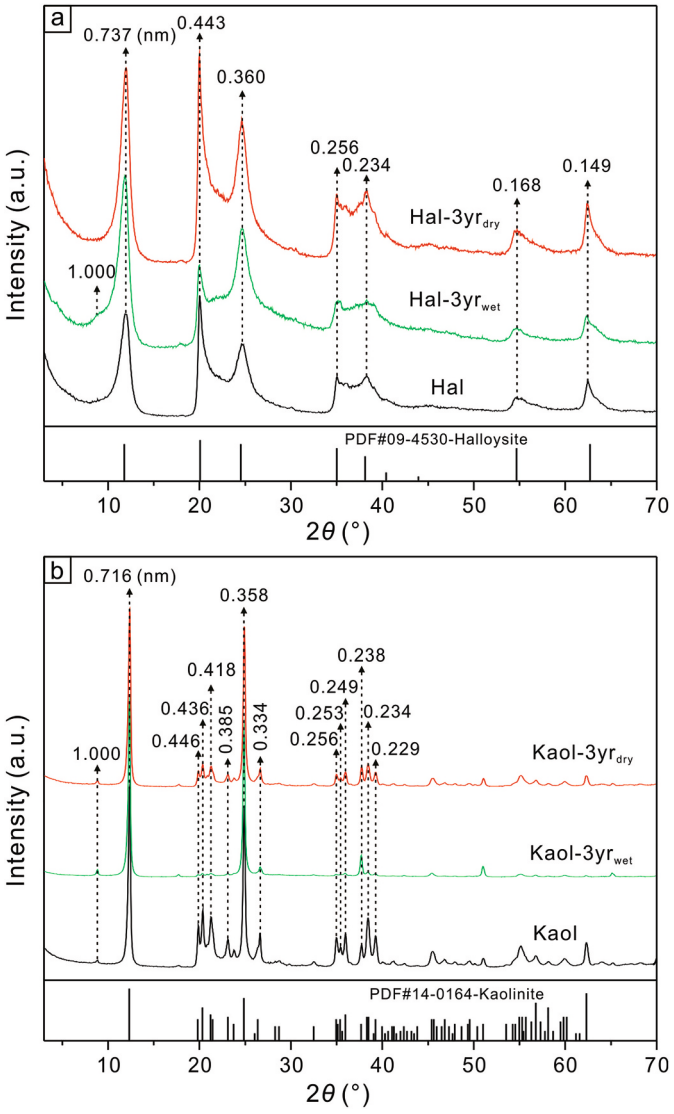

Fig. 1. XRD patterns of Hal, Hal-3yr$_{wet}$, and Hal-3yr$_{dry}$ (a); XRD patterns of Kaol, Kaol-3yr$_{wet}$, and Kaol-3yr$_{dry}$ (b).

The La(III) aqueous solution was prepared using $La(NO_3)_3$ of analytical grade, obtained from Shanghai Macklin Biochemical Co., Ltd. Its concentration was 1×10^{-4} mol/L, similar to the mean concentration of various cations in groundwater (Huang et al., 2013). The solution's pH was 5, corresponding to that of typical WED-RE ores (Estrade et al., 2019; Yang et al., 2019). Ultra-pure water (18.25 MΩ cm^{-1}) was used throughout the experiment.

2.2. Analytical methods

The wet halloysite (Hal-3yr$_{wet}$) and kaolinite (Kaol-3yr$_{wet}$) that underwent the 3-year-long immersion were measured by XRD, using a diffractometer of the Rigaku Corporation (Japan) with Cu Kα radiation (λ = 0.154 nm) generated at 40 kV and 250 mA. The specimens were

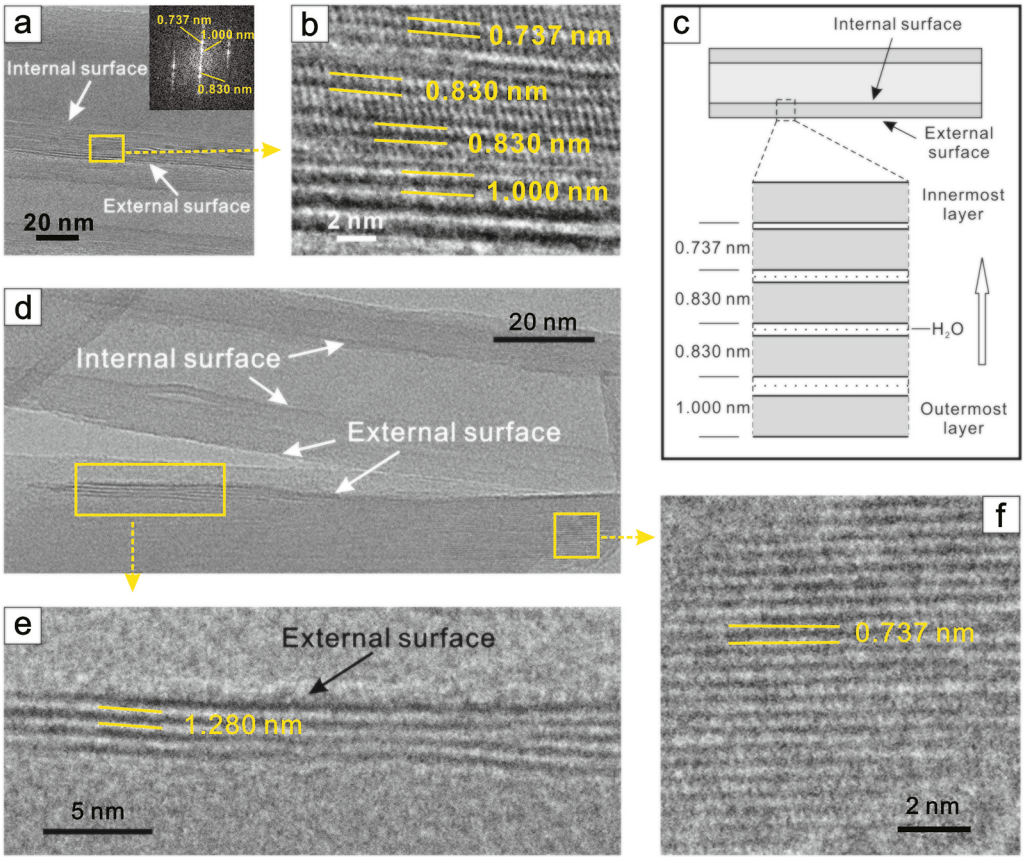

Fig. 2. (a) TEM image of Hal-3yr$_{wet}$ and the inset is the fast Fourier transform (FFT) pattern of the yellow rectangle in (a); (b) HRTEM image of the yellow rectangle in (a); (c) a schematic diagram of distribution features of the enlarged layers in rehydrated tubular halloysite; (d) TEM image of Hal-3yr$_{wet}$; (e) and (f) the magnification of the yellow rectangle and square, respectively. (For interpretation of the references to colour in this figure legend, the reader is referred to the web version of this article.)

investigated from 3° to 70° (2θ) with a scanning speed of 4° per minute. Next, both Hal-3yr$_{wet}$ and Kaol-3yr$_{wet}$ were dried at 60 °C (hereon Hal-3yr$_{dry}$ and Kaol-3yr$_{dry}$, respectively) and were measured again by XRD.

The TEM images, high-resolution TEM (HRTEM) images, high-angle annular dark-field scanning transmission electron microscopy (HAADF-STEM) images, and energy-dispersive X-ray (EDX) spectroscopy were all collected using a FEI Talos F200s field-emission TEM operating at an accelerating voltage of 200 kV. The Hal, Hal-3yr$_{wet}$, and Hal-3yr$_{dry}$ were ultrasonically dispersed in ultra-pure water for 6 min, respectively, and then two droplets of each suspension were dropped onto a carbon-coated copper grid to prepare the specimens for their TEM observation. The specimens of Kaol and Kaol-3yr$_{wet}$ were prepared using Leica EM UC7 Ultramicrotome, by following the method of Liu et al. (2019).

Fourier transform infrared spectroscopy (FTIR) of Hal, Hal-3yr$_{dry}$, Kaol, and Kaol-3yr$_{dry}$ were recorded by a Bruker Vertex 70 IR spectrometer. The specimens were prepared by mixing 0.9 mg of each sample and 80 mg of KBr, followed by pressing the mixtures into pellets. A pure KBr pellet was measured as the background. All spectra were collected over 64 scans in the range of 4000–400 cm^{-1} at a resolution of 4 cm^{-1}. Meanwhile, attenuated total internal reflectance Fourier transform infrared spectroscopy (ATR-FTIR) of the concentrated suspensions was conducted using the same IR spectrometer, but equipped with a multibounce horizontal ATR accessory and flow cell (Pike Technologies) (Liu et al., 2016), to reveal the structural characteristics of Hal-3yr$_{wet}$ and Kaol-3yr$_{wet}$.

The La chemical state of Hal-3yr$_{dry}$ and Kaol-3yr$_{dry}$ were respectively characterized by a K-Alpha X-ray photoelectron spectrometer (Thermo Fisher Scientific, UK) with a monochromatic Al K X-ray source (excitation energy = 1468.6 eV). The spectra were collected from 0 to 1350 eV, with an X-ray spot size of 400 μm. The binding energies were corrected relative to the carbon 1 s signal at 284.8 eV.

3. Results

3.1. Structure and morphology of halloysite and kaolinite before and after their aging

The XRD patterns of Hal, Hal-3yr$_{wet}$, and Hal-3yr$_{dry}$ are shown in Fig. 1a. For Hal, its *d*-values were 0.737, 0.443, 0.360, 0.168, and 0.149 nm (Fig. 1a), corresponding to the (001), (100), (002), (210), and (300) reflections of halloysite (7 Å), which suggests high-purity halloysite was used in this study. In the XRD pattern of Hal-3yr$_{wet}$, a weak shoulder peak appeared at ~1.000 nm, which was ascribed to the (001) reflection of halloysite (10 Å) (Du et al., 2018). The low intensity of the (001) reflection at ~1.000 nm suggested the minority of halloysite (10 Å) in Hal-3yr$_{wet}$, with halloysite (7 Å) in the majority. The weak (001) reflection at ~1.000 nm disappeared in Hal-3yr$_{dry}$ (Fig. 1a) due to the dehydration of halloysite (10 Å). Compared with the (100) reflection of Hal, Hal-3yr$_{wet}$, and Hal-3yr$_{dry}$, the intensity of the (100) reflection in Hal-3yr$_{wet}$ was diminished. For both halloysite (7 Å) and halloysite (10 Å), their peak at 0.443 nm was ascribed to the (100) reflection; this suggested the reduced intensity arose from the orientation during specimen preparation rather than the presence of halloysite (10 Å).

The XRD patterns (Fig. 1b) of Kaol before and after the aging process (i.e., 3-year-long immersion) were nearly the same. Almost all reflections were indexed to be kaolinite, having a d_{001}-value of 0.716 nm. The weak peak at 1.000 nm was the typical (001) reflection of illite (Drits et al., 2010), an impurity commonly existing in natural kaolinite. Similar to Hal-3yr$_{wet}$, Kaol-3yr$_{wet}$ also displayed some reflections of reduced intensity due to the orientation, such as those at 0.446, 0.436, 0.418, 0.385, 0.256, 0.249, 0.238, 0.234, and 0.229 nm.

The TEM and HRTEM images of Hal-3yr$_{wet}$ are shown in Fig. 2. The (001) layer stacks of Hal-3yr$_{wet}$ were slightly disordered, as indicated by the FFT pattern and the HRTEM (Fig. 2a and b). Notably, Fig. 2b shows

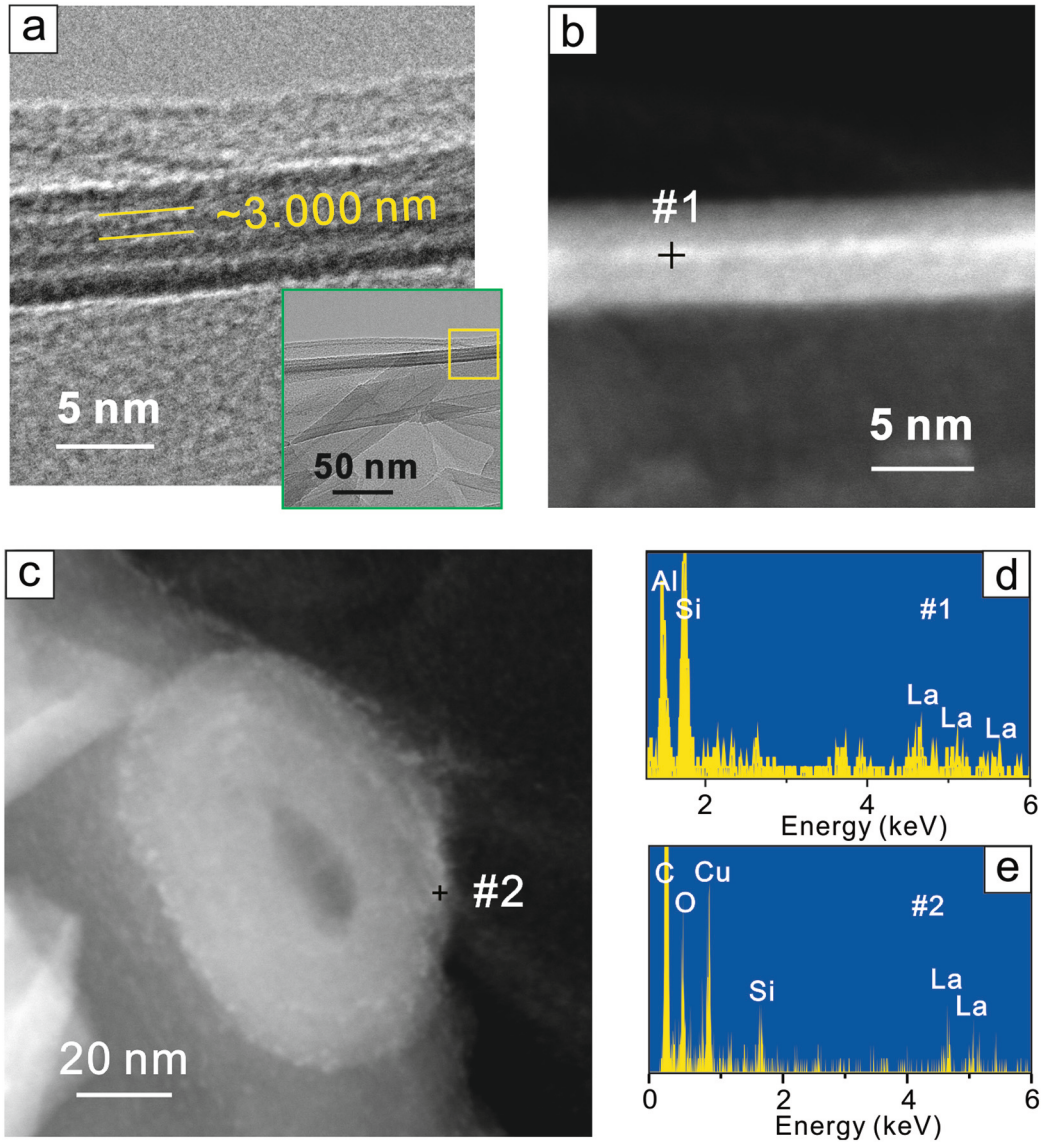

Fig. 3. HRTEM (a) and HAADF (b) images of interlayer's La-bearing particles in Hal-3yr$_{wet}$; (c) HAADF image of La-bearing particles on the surface of halloysite in Hal-3yr$_{wet}$; (d) and (e) the EDS results of spot #1 and spot #2, respectively.

the lattice fringes of ~1.000 and ~0.830 nm in Hal-3yr$_{wet}$ (Fig. 2b), which demonstrated the formation of partially hydrated halloysite, consistent with the XRD analysis results in Fig. 1a. It should also be noted that the lattice fringes of 1.000 nm always appeared at the outermost layers of halloysite nanotubes and those of 0.830 nm appeared near the outermost layers of the nanotubes (Fig. 2b and c). Meanwhile, there were also some layers with the $d_{(001)}$-value of 1.280 nm at the outermost layers of the halloysite (Fig. 2d). Moreover, Fig. 3a shows the lattice fringes of ~3.000 nm, which could have originated from the interlayer's La-bearing particles (Fig. 3b and d). In addition to the interlayer, La-bearing nanosized particles were also found distributed on the surface of halloysite (Fig. 3c and e).

After drying the Hal-3yr$_{wet}$, the lattice fringes of ~0.830 and ~1.000 nm disappeared in Hal-3yr$_{dry}$ (Fig. 4a), which corresponded to the disappearance of the (001) reflection of halloysite (10 Å) in Hal-3yr$_{dry}$ (Fig. 1a). By contrast, no significant differences in the structure and morphology of Hal and Hal-3yr$_{dry}$ were found (Fig. 4a and d).

Cross-sectional HRTEM images of Kaol-3yr$_{wet}$ and Kaol appear in Fig. 4. They suggested these two samples had the same mineralogical structure, both having the $d_{(001)}$-value of 0.716 nm. These results further indicated that the microstructure of kaolinite went largely unchanged during its long-term immersion, in agreement with the XRD analysis results (Fig. 1b).

3.2. IR results

The ATR-FTIR spectra of wet Hal (Hal$_{wet}$), Hal-3yr$_{wet}$, wet Kaol (Kaol$_{wet}$), and Kao-3yr$_{wet}$ are shown in Fig. 5a. The assignments for each of their corresponding vibrational modes observed are compiled in Table 1, based on previous reports (Frost and Vassallo, 1996; Tan et al., 2015; Yang et al., 2012; Yariv and Shoval, 1976; Yuan et al., 2008). In the OH stretching region of Hal$_{wet}$, there were two IR vibration bands at 3695 and 3621 cm^{-1}, which arose from the coupled stretching vibrations of nonequivalent inner-surface OH groups and the stretching vibrations of single inner hydroxyl groups, respectively (Madejová et al., 2017). Nevertheless, some new bands, such as the OH stretching of inner-surface hydroxyl groups at ~3682 cm^{-1} and ~3658 cm^{-1}, appeared in Hal-3yr$_{wet}$. Evidently, when compared with the ATR-FTIR spectra of Hal$_{wet}$ and Hal-3yr$_{wet}$, the intensity of the band at 3697 cm^{-1} in Hal-3yr$_{wet}$ increased (Fig. 5a). For Kaol$_{wet}$, in addition to that detected at 3694 and 3620 cm^{-1}, there was also a vibration band at 3654 cm^{-1} (Fig. 5a), similar to previous research (Chen et al., 2017). In

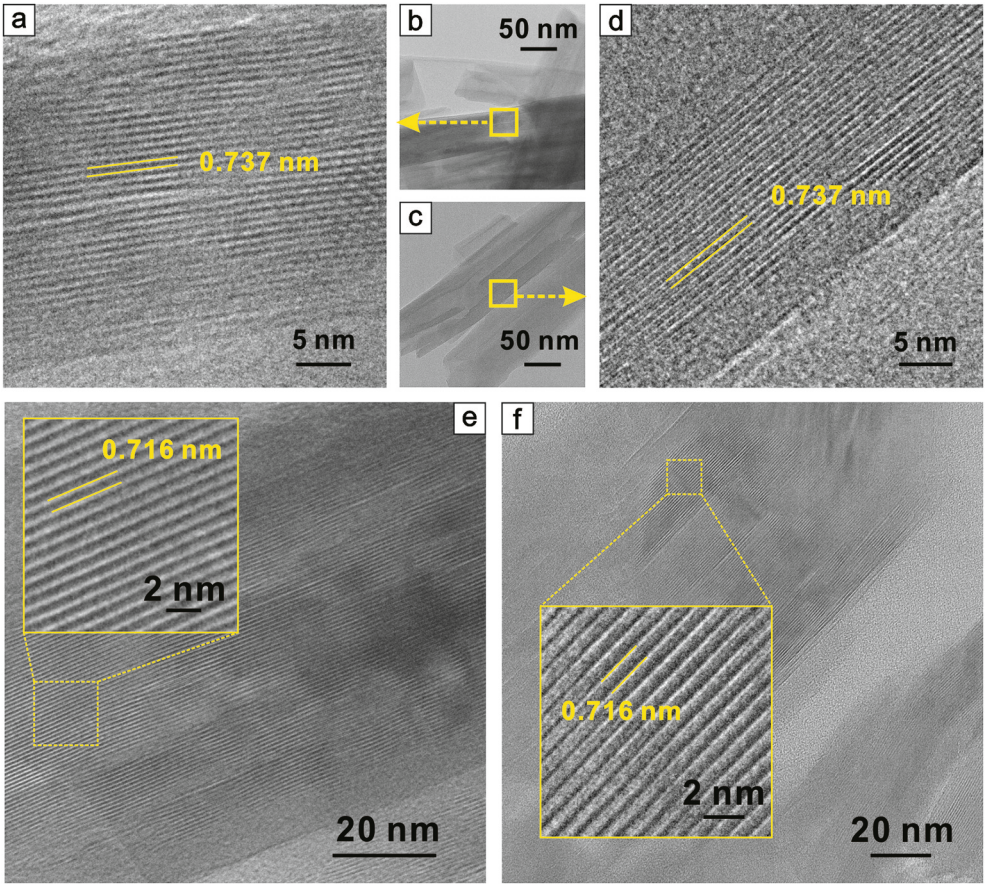

Fig. 4. TEM and HRTEM images of Hal-3yr$_{dry}$ (a and b), Hal (c and d), Kaol-3yr$_{wet}$ (e), and Kaol (f).

the ATR-FTIR spectrum of Kaol-3yr$_{wet}$, this band (at 3654 cm^{-1}) split into two vibration bands (~3666 and 3656 cm^{-1}).

Fig. 5b displays the FTIR spectra of Hal, Hal-3yr$_{dry}$, Kaol, and Kaol-3yr$_{dry}$. Hal and Hal-3yr$_{dry}$ each had two bands at 3695 and 3620 cm^{-1} in the OH stretching region. The spectrum of Hal-3yr$_{dry}$ closely resembled that of Hal (Fig. 5b), illustrating that these two samples had very similar structures. The FTIR spectra of Kaol and Kaol-3yr$_{dry}$ revealed four resolved bands at 3695, 3669, 3654, and 3620 cm^{-1} in the OH stretching region (Fig. 5b). Similarly, Kaol and Kaol-3yr$_{dry}$ had the same pattern of FTIR spectra, thus demonstrating the same structure of these two samples.

3.3. The XPS spectra of La

The characterization of chemical species of La 3d$_{5/2}$ onto the Hal-3yr$_{dry}$ and Kaol-3yr$_{dry}$ is depicted in Fig. 6 and summarized in Table 2. The spin-orbit component can be split via multiplet splitting (Fig. 6). The peak with higher binding energy was the satellite of La 3d$_{5/2}$, resulting from the bonding and antibonding states between the $3d^94f^0$ and $3d^94f^1\underline{L}$ configurations (Suga et al., 1996). Three conspicuous features in the La 3d$_{5/2}$ spectra of Hal-3yr$_{dry}$ and Kaol-3yr$_{dry}$ (Fig. 6) indicated three different chemical species of La.

The peaks at 836.79 and 837.40 eV in the La XPS spectra of Hal-3yr$_{dry}$ (Fig. 6a) were similar to the XPS characteristics of La-bearing zeolites (Grunert et al., 1993), in which La^{3+} ions exchanged Na^{+} ions and entered into the extra framework cages of zeolite (Tian et al., 2006). La(III) ions in the zeolites exist as free ions (i.e., outer-sphere complexes) and complexes with Al(Si)-OH (Lee and Valla, 2017). Therefore, the peaks at 836.79 and 837.40 eV in the XPS spectrum of Hal-3yr$_{dry}$ were associated with the inner-sphere complexes and outer-sphere complexes, respectively. Similarly, the peaks at 836.84 and 837.43 eV in the La XPS spectrum of Kaol-3yr$_{dry}$ (Fig. 6b) corresponded to inner-sphere complexes and outer-sphere complexes.

Further, another peak with low binding energy at 835.50 eV in the XPS spectrum of Hal-3yr$_{dry}$ had a spin-orbit splitting (ΔE) of 3.59 eV, this being rather close to the distinguishing feature of the compound La(OH)$_3$ or LaO(OH) (Li et al., 2019a), which suggested the La-bearing particles in Fig. 3 were La hydroxides. Similarly, for Kaol-3yr$_{dry}$, the binding energy at 835.62 eV with the spin-orbit splitting of 3.60 eV was also ascribed to La hydroxides particles. As suggested by previous research (Fleisch et al., 1984; Fleming et al., 2010), the LaO(OH) particles generally formed from the dehydration of La(OH)$_3$.

4. Discussion

4.1. Chemical state of La(III) on the halloysite and kaolinite

The XPS results (Fig. 6), there revealed three different chemical states of La in the samples: outer-sphere complexes, inner-sphere complexes, and La hydroxides. Previous REE(III) adsorption experiments found that halloysite and kaolinite could primarily adsorb REE(III) ions via the outer-sphere complexation and inner-sphere complexation (Coppin et al., 2002; Yang et al., 2019), of which the latter was the predominant adsorption mechanism (Yang et al., 2019). As seen in Table 2, the atomic ratio between inner-sphere complexes (836.84 eV) and outer-sphere complexes (837.43 eV) of La(III) was 1.545 for Kaol-3yr$_{dry}$; however, the ratio was just 0.790 for Hal-3yr$_{dry}$, which means the outer-sphere complexes were the primary La species compared with inner-sphere complexes in Hal-3yr$_{dry}$. This specular ratio in Hal-3yr$_{dry}$ is likely associated with the structural changes of Hal; i.e., the transformation of halloysite (7 Å) to halloysite (10 Å), after the 3-year-long immersion in La(III) aqueous solution.

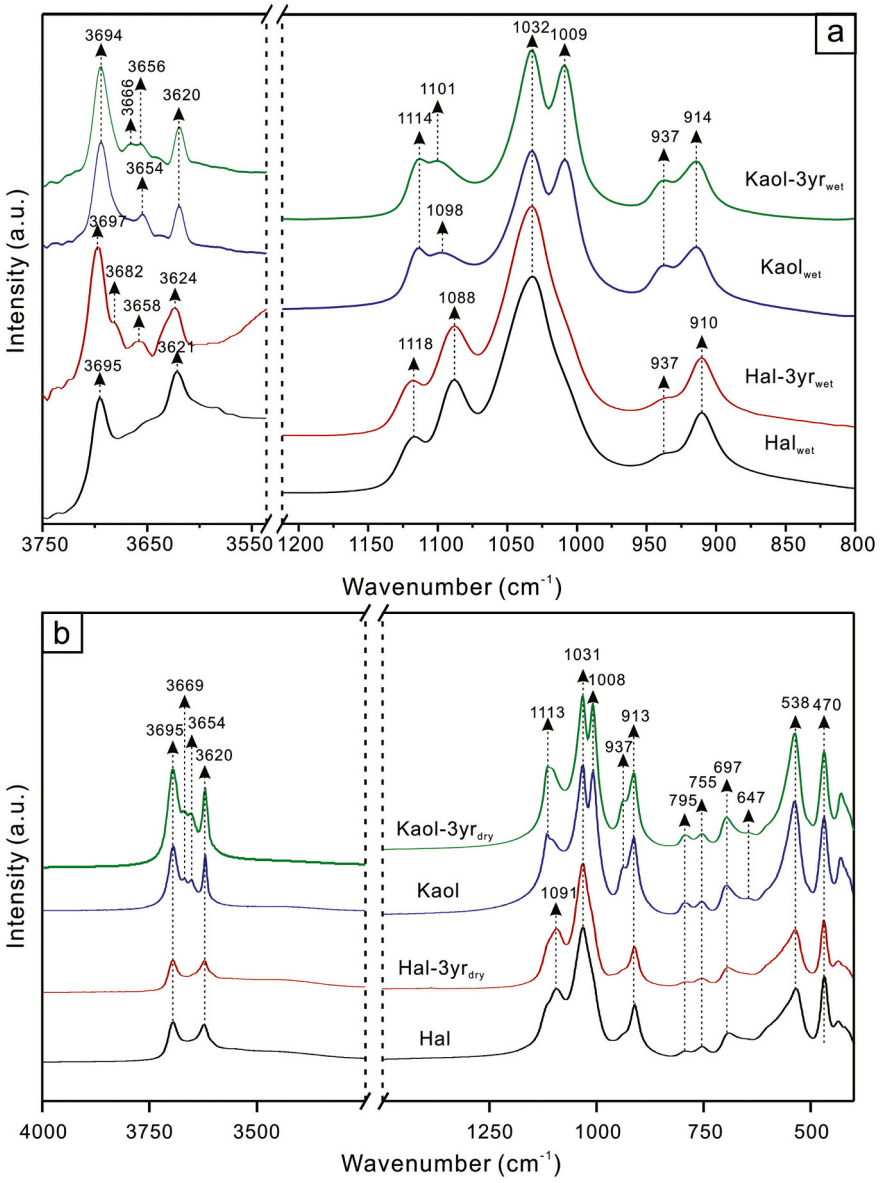

Fig. 5. ATR-FTIR patterns (a) of Hal$_{wet}$, Hal-3yr$_{wet}$, Kaol$_{wet}$, and Kaol-3yr$_{wet}$; FTIR patterns (b) of Hal, Hal-3yr$_{dry}$, Kaol, and Kaol-3yr$_{dry}$.

Table 1
Positions and assignment of the IR vibration bands.

Position (cm^{-1})	Assignments
470	Deformation of Si-O-Si
538	Deformation of Al-O-Si
697	Perpendicular Si-O stretching
755	Perpendicular Si-O stretching
795	Symmetric stretching of Si-O
913/914	O-H deformation of inner hydroxyl groups
937	O-H deformation of inner-surface hydroxyl groups
1008/1009	in-plane Si-O stretching
1031/1032	in-plane Si-O stretching
1088/1091	in-plane Si-O stretching
1101/1098	perpendicular Si-O stretching
1113/1114/1118	perpendicular Si-O stretching
3620/3621/3624	O-H stretching of inner hydroxyl groups
3654/3656/3658	O-H stretching of inner-surface hydroxyl groups
3666/3669	O-H stretching of inner-surface hydroxyl groups
3682	O-H stretching of inner-surface hydroxyl groups
3694/3695/3697	O-H stretching of inner-surface hydroxyl groups

The $d_{(001)}$-value of 1.280 nm in the Hal-3yr$_{wet}$, which is significantly larger than that for the interlayer with a monolayer of water molecules ($d_{(001)}$-value of 1.000 nm) (Jemai et al., 1999; Joussein et al., 2006), indicates that La(III) ions migrated into the interlayer of halloysite. In an aqueous solution environment, La(III) ions always form hydrated ions, whose coordination number of water molecules commonly is 9 for the first hydration shell (D'Angelo et al., 2011; Duvail et al., 2007). The average La-O distance of the first hydration shell was approximately 0.252–0.259 nm (D'Angelo et al., 2011; Duvail et al., 2007), suggesting the hydrated La(III) ions have a diameter over 0.500 nm and could give rise to the lattice fringe of ~1.280 nm (Figs. 2d and 7). Moreover, the occurrence of an interlayer La hydroxides (Fig. 3b) also implies the La (III) ions can enter into the interlayer of halloysite.

For halloysite (10 Å), Yariv and Shoval (1976) found the in-phase coupled O-H stretching vibration at ~3700 cm^{-1} shifted to 3688 or 3685 cm^{-1} when cations (e.g., Cs^+ and Rb^+) entered into the interlayer. Likewise, the OH stretching vibration at 3682 cm^{-1} in Hal-3yr$_{wet}$ (Fig. 5a) shifted from 3695 cm^{-1}, pointing to the presence of interlayer La(III) ions. That red shift was mainly driven by the hydrogen bonds (Joseph and Jemmis, 2007) between the interlayer La(III), water

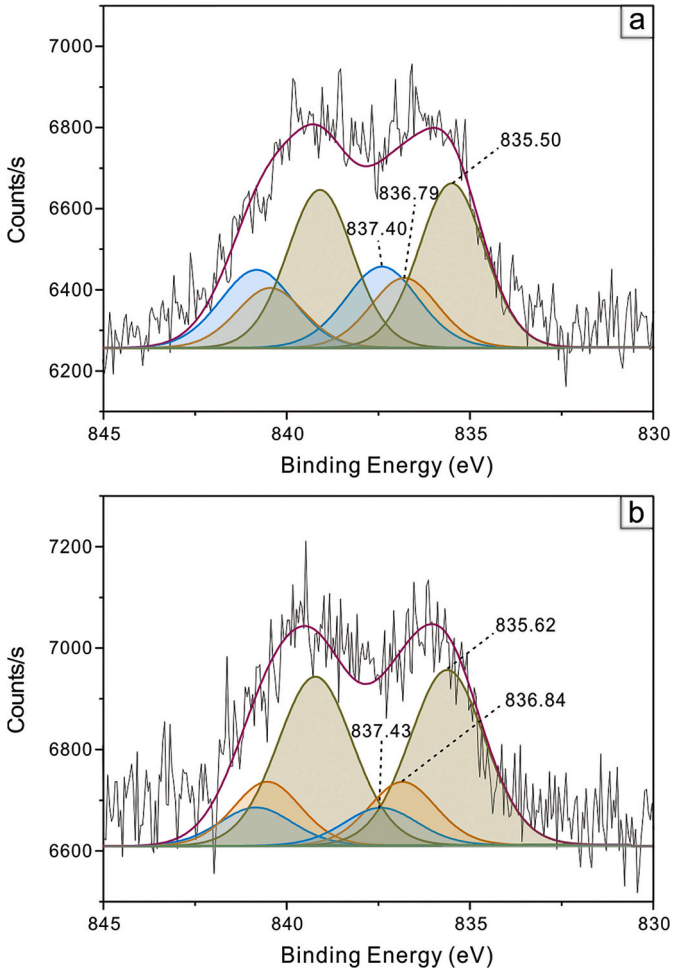

Fig. 6. XPS spectra of Hal-3yr$_{dry}$ (a) and Kaol-3yr$_{dry}$ (b).

Table 2
La $3d_{5/2}$ binding energy (eV) and relative content of various features of La on halloysite and kaolinite.

Samples	La $3d_{5/2}$ BE(eV)		ΔE (eV)	Relative content (%)
	Peak	Satellite		
Hal-3yr$_{dry}$	835.50	839.09	3.59	50.36
	836.79	840.45	3.66	21.91
	837.40	840.82	3.42	27.73
Kaol-3yr$_{dry}$	835.62	839.22	3.6	65.24
	836.84	840.53	3.69	21.10
	837.43	840.84	3.41	13.66

molecules, and OH groups. The weakened and lengthened bond of the OH stretching vibration at ~3697 cm^{-1} caused by hydrogen bonds could also have intensified the band at 3697 cm^{-1} (Fig. 5a) (Joseph and Jemmis, 2007). Recently, Hillier et al. (2016) observed the bands near 3670 and 3653 cm^{-1} in prismatic halloysite, also arising from the hydrogen bonds (Madejová et al., 2017), which supports our inference that the band near 3658 cm^{-1} (Fig. 5a) was also due to hydrogen bonds.

Accordingly, undergoing long-time immersion, La(III) ions were not only adsorbed on the surface of tubular halloysite by inner-sphere complexation and outer-sphere complexation, but they also penetrated the interlayer of tubular halloysite (Fig. 7). These interlayer La(III) ions mainly existed as outer-sphere complexes, accounting for the higher content of outer-sphere complexes than inner-sphere complexes (Table 2). Notably, the extent and scale of the intercalation corresponding to the lattice fringes of ~1.280 and 1.000 nm is difficult to assess, because of the small and selective field of view for TEM observation. Finally, since other REE(III) ions have similar chemical properties to La(III) ion but a smaller radius than it, the results of our study suggest REE(III) ions can move into the interlayer of tubular halloysite, which thereby suggests a new possible state of REE(III) occurrence in WED-RE ores.

4.2. Partial rehydration of tubular halloysite (7 Å)

Generally, halloysite in weathered crusts has two forms: dehydrated halloysite (i.e., halloysite (7 Å), $Al_2(OH)_4Si_2O_5$) (Chen et al., 2020; Estrade et al., 2019; Yang et al., 2019) and hydrated halloysite (i.e., halloysite (10 Å), $Al_2(OH)_4Si_2O_5{\cdot}2H_2O$) (Estrade et al., 2019; Li and Zhou, 2020; Li et al., 2020; Ram et al., 2019). Both are considered the end-members of a continuous series of hydration states (Joussein et al., 2006; Slansky, 1985). In halloysite (10 Å), one layer of water molecules between the multilayers gives rise to a d_{001}-value of 1.000 nm (Jemai et al., 1999; Joussein et al., 2006). Halloysite (7 Å) is easily obtained through the loss of those interlayer water molecules under a dry air and/or mildly hot environment, and this dehydration is deemed to be an irreversible process (Joussein et al., 2005; Yuan et al., 2015; Yuan, 2016). Once the interlayer water is lost, it cannot be restored by treatment with water (Giese, 1988; Joussein et al., 2006). For example, Joussein et al. (2006) immersed tubular halloysite (7 Å) in water for 3 months but its structure did not change significantly.

Intriguingly, our results demonstrated that partial rehydration of tubular halloysite (7 Å) could occur, to form partially hydrated halloysite in La(III) solution, as implied by the weak shoulder peak at ~1.000 nm in the XRD pattern (Fig. 1) and the lattice fringes of ~0.830 and ~1.000 nm in the HRTEM images (Fig. 2) of Hal-3yr$_{wet}$. The lattice fringe of ~1.000 nm was due to the presence of interlayer water molecules, including two types of them located at 3 Å and 3.4 Å from the hydroxyl surface over the octahedral sheet (Jemai et al., 1999; Joussein et al., 2006). The lattice fringes of ~0.830 nm (Fig. 2b) generally belonged to an intermediate product, in which the water molecule was inserted between vacant octahedral site and ditrigonal cavity of the tetrahedral sheet (Joussein et al., 2006). Moreover, the distribution features of the lattice fringes with $d_{(001)}$-value of 1.000 nm and 0.830 nm (Fig. 2c) indicate that the rehydration initially occurs at the outermost layers of halloysite (7 Å) and then extends to its internal surface.

Despite the reason for the rehydration of halloysite (7 Å) being largely unclear at this stage, it is very likely relevant to the interactions between the adjacent layers of a halloysite nanotube. Based on an ab initio simulation of kaolinite structure, Benco et al. (2001) found that the kaolinite structure had the lowest total energy as its d_{001}-value is 0.740–0.780 nm, which implies weak interactions between layers; further, those with the d_{001}-value of ~0.740 nm could be easily intercalated by small molecules such as water molecules (Benco et al., 2001). Their finding concurs with the rehydration reported here for tubular halloysite (7 Å) (d_{001}-value of 0.737 nm) but not kaolinite (d_{001}-value of 0.716 nm) (Fig. 1a). Besides, the structural stress induced from the misfit of the tetrahedral and octahedral sheets may be another possible factor influencing the intercalation (Deng et al., 2002). For tubular halloysite with the spiral structure, the curvature decreases from the innermost layer to the outermost layer (Ferrante et al., 2015). Consequently, the structural stress in the layer dominated by cation–cation Coulomb repulsion (e.g., Si-Si in the tetrahedral sheet) (Singh, 1996), is slightly weaker in the outermost than innermost layer. This difference in the structural stress of the layer at different positions of the halloysite nanotube may explain why the rehydration initially occurred at the outermost layers.

That La(III) induced intercalation of halloysite (7 Å) is highly relevant for the ionic properties, e.g., radius and hydration energy. Previous studies have pointed out that interlayer cations (e.g, Ca^{2+}) are generally considered to play a key role in the hydration process of halloysite (Bailey, 1990; Joussein et al., 2006). Joussein et al. (2006) discussed

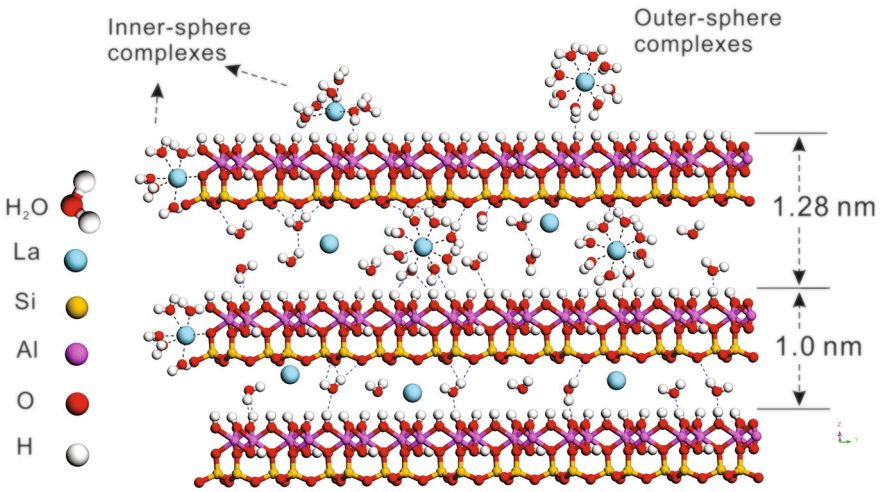

Fig. 7. A schematic diagram of the inner-sphere complexes and outer-sphere complexes of La(III) ions in Hal-3yr$_{wet}$.

how Ca^{2+} and K^{+} ions affect the rehydration of spheroidal halloysite (7 Å). The Ca-saturated spheroidal halloysite (7 Å) undergoing a 3-month-long immersion could partially rehydrate and form spheroidal halloysite (10 Å), whereas there was no discernible change for the K-saturated sample (Joussein et al., 2006). This difference was closely associated with the ionic radius (0.99 and 1.33 Å for Ca^{2+} and K^{+}, respectively) and hydration energy (−1515 and −304 kJ/mol for Ca^{2+} and K^{+}, respectively) of the interlayer Ca^{2+} and K^{+} ions. Therefore, the hydration of halloysite was probably dominated by the affinity of cations for water molecules (Joussein et al., 2006). The La(III) ions have a radius of 1.06 Å and a hydration energy of −3285 kJ/mol (Moldoveanu and Papangelakis, 2012). Consequently, the La(III) ions have a greater affinity for water than does Ca^{2+} yet a similar ionic radius to Ca^{2+}, which suggests the occurrence of interlayer La(III) could facilitate the rehydration of tubular halloysite (7 Å). In addition to those hydrated La(III) ions in the interlayer with a $d_{(001)}$-value of 1.280 nm (Fig. 7), the La(III) in interlayer with the $d_{(001)}$-value of 1.000 nm might be associated with "hole" water, not unlike Ca^{2+} is (Joussein et al., 2006).

In the groundwater, there are some cations (e.g., Na^{+}) that have a smaller ionic radius than does La(III) (Joussein et al., 2006; Moldoveanu and Papangelakis, 2012). Therefore, our results suggest that the rehydration of halloysite (7 Å) could be a common phenomenon under the long-term effects of contact exposure to groundwater. For example, there is more halloysite (10 Å) in the deeper horizon of the weathered profile in WED-RE ores (Li and Zhou, 2020). In addition, the rehydration of halloysite might be also associated with its formation mechanism and environment, resulting in differences in its characteristics, such as the morphology and chemical composition (Cavallaro et al., 2018; Joussein et al., 2005; Yuan et al., 2019). Given that halloysite (10 Å) typically has a higher cation exchange capacity (CEC) than halloysite (7 Å) (Joussein, 2016; Yaraghi et al., 2020), the occurrence of halloysite (10 Å) should be conducive to the enrichment of exchangeable REE(III) ions in WED-RE ores (Ram et al., 2019), as well as the deprotonation of clay minerals under the influence of pH (Yang et al., 2019).

5. Conclusion

After its 3-year-long immersion in La(III) aqueous solution, the tubular halloysite (7 Å) was partially rehydrated, forming the hydrated halloysite; whereas, such rehydration did not occur for kaolinite. Distribution features of the lattice fringes of 1.000 nm and 0.830 nm indicated the rehydration process very likely began at the external surface of halloysite (7 Å) at first. The rehydration of tubular halloysite in La(III) solution advances our understanding of the stability and structure of halloysite (7 Å).

In rehydrated halloysite, La(III) ions not only existed as inner-sphere complexes, outer-sphere complexes, and hydroxide particles adsorbed on the surface, but they also entered the interlayer of the mineral. The interlayer La(III) ions primarily consist of outer-sphere complexes and so they play a pivotal role in halloysite rehydration. Due to the similar chemical properties of REE(III) to La(III), the results of this work suggest that long-term interaction enables REE(III) ions to penetrate the interlayer of halloysite with long-term interaction, thereby revealing a new possible state of REE(III) occurrence in weathered crusts.

Credit author statement

All persons who meet authorship criteria are listed as authors, and all authors certify that they have participated sufficiently in the work.

Declaration of Competing Interest

The authors declare that they have no known competing financial interests or personal relationships that could have appeared to influence the work reported in this paper.

Acknowledgments

Financial supports from the National Special Support for High-Level Personnel and the National Natural Science Foundation of China (Grant No. 41672042 and 41972045) are gratefully acknowledged. This is a contribution No. IS-3060 from GIGCAS.

References

Bailey, S.W., 1990. Halloysite - A critical assessment. In: Farmer, V.C., Tardy, Y. (Eds.), Surface Chemistry Structure and Mixed Layering of Clays. Proceedings of the 9th International Clay Conference, Strasbourg, 1989, II, pp. 89–98.
Bao, Z.W., Zhao, Z.H., 2008. Geochemistry of mineralization with exchangeable REY in the weathering crusts of granitic rocks in South China. Ore Geol. Rev. 33, 519–535.
Bau, M., 1999. Scavenging of dissolved yttrium and rare earths by precipitating iron oxyhydroxide: Experimental evidence for Ce oxidation, Y-Ho fractionation, and lanthanide tetrad effect. Geochim. Cosmochim. Acta 63 (1), 67–77.
Benco, L., Tunega, D., Hafner, J., Lischka, H., 2001. Upper limit of the O-H center dot center dot center dot O hydrogen bond. Ab initio study of the kaolinite structure. J. Phys. Chem. B 105, 10812–10817.
Borst, A.M., Smith, M.P., Finch, A.A., Estrade, G., Villanova-de-Benavent, C., Nason, P., Marquis, E., Horsburgh, N.J., Goodenough, K.M., Xu, C., Kynicky, J., Geraki, K., 2020. Adsorption of rare earth elements in regolith-hosted clay deposits. Nat. Commun. 11.
Cavallaro, G., Chiappisi, L., Pasbakhsh, P., Gradzielski, M., Lazzara, G., 2018. A structural comparison of halloysite nanotubes of different origin by Small-Angle Neutron Scattering (SANS) and electric birefringence. Appl. Clay Sci. 160, 71–80.
Chakhmouradian, A.R., Wall, F., 2012. Rare earth elements: minerals, mines, magnets (and more). Elements 8, 333–340.

Chen, H.F., Koopal, L.K., Xiong, J., Avena, M., Tan, W.F., 2017. Mechanisms of soil humic acid adsorption onto montmorillonite and kaolinite. J. Colloid Interface Sci. 504, 457–467.
Chen, L.K., Jin, X.W., Chen, H.X., He, Z.W., Qiu, L.R., Duan, H.R., 2020. Grain size distribution and clay mineral distinction of rare earth ore through different methods. Minerals 10, 27.
Chi, R.A., Tian, J., Luo, X.P., Xu, Z.G., He, Z.Y., 2012. The basic research on the weathered crust elution-deposited rare earth ores. Nonferr. Metals Sci. Eng. 3 (4), 1–13.
Coppin, F., Berger, G., Bauer, A., Castet, S., Loubet, M., 2002. Sorption of lanthanides on smectite and kaolinite. Chem. Geol. 182 (1), 57–68.
D'Angelo, P., Zitolo, A., Migliorati, V., Chillemi, G., Duvail, M., Vitorge, P., Abadie, S., Spezia, R., 2011. Revised ionic radii of Lanthanoid(III) ions in aqueous solution. Inorg. Chem. 50, 4572–4579.
Deng, Y.J., White, G.N., Dixon, J.B., 2002. Effect of structural stress on the intercalation rate of kaolinite. J. Colloid Interface Sci. 250, 379–393.
Dodds, W.K., Whiles, M.R., 2020. Properties of water. In: Dodds, W.K., Whiles, M.R. (Eds.), Freshwater Ecology, 3rd ed. Academic Press, pp. 21–48.
Drits, V.A., Zviagina, B.B., McCarty, D.K., Salyn, A.L., 2010. Factors responsible for crystal-chemical variations in the solid solutions from illite to aluminoceladonite and from glauconite to celadonite. Am. Mineral. 95, 348–361.
Du, P.X., Liu, D., Yuan, P., Deng, L.L., Wang, S., Zhou, J.M., Zhong, X.M., 2018. Controlling the macroscopic liquid-like behaviour of halloysite-based solvent-free nanofluids via a facile core pretreatment. Appl. Clay Sci. 156, 126–133.
Duvail, M., Spezia, R., Cartailler, T., Vitorge, P., 2007. Temperature dependence of hydrated La3+ properties in liquid water, a molecular dynamics simulations study. Chem. Phys. Lett. 448, 41–45.
Estrade, G., Marquis, E., Smith, M., Goodenough, K., Nason, P., 2019. REE concentration processes in ion adsorption deposits: evidence from the Ambohimirahavavy alkaline complex in Madagascar. Ore Geol. Rev. 112.
Ferrante, F., Armata, N., Lazzara, G., 2015. Modeling of the halloysite spiral nanotube. J. Phys. Chem. C 119, 16700–16707.
Fleisch, T.H., Hicks, R.F., Bell, A.T., 1984. An XPS study of metal support interactions Pd/SiO_2 AND Pd/La_2O_3. J. Catal. 87, 398–413.
Fleming, P., Farrell, R.A., Holmes, J.D., Morris, M.A., 2010. The rapid formation of La $(OH)_3$ from La_2O_3 powders on exposureto water vapor. J. Am. Ceram. Soc. 93, 1187–1194.
Frost, R.L., Vassallo, A.M., 1996. The dehydroxylation of the kaolinite clay minerals using infrared emission spectroscopy. Clay Clay Miner. 44, 635–651.
Galán, E., Ferrell, R.E., 2013. Genesis of clay minerals. In: Bergaya, F., Lagaly, G. (Eds.), Handbook of Clay Science, 5. Elsevier, pp. 83–126.
Garcia, M.V.R., Krzemien, A., del Campo, M.A.M., Alvarez, M.M., Gent, M.R., 2017. Rare earth elements mining investment: it is not all about China. Res. Policy 53, 66–76.
Giese, R.F., 1988. Kaolin minerals: structures and stabilities. In: Bailey, S.W. (Ed.), Hydrous Phyllosilicates (Exclusive of Micas). Review in Mineralogy, 19. Mineralogical Society of America, Chelsea, MI, pp. 29–66.
Gleeson, T., Befus, K.M., Jasechko, S., Luijendijk, E., Cardenas, M.B., 2016. The global volume and distribution of modern groundwater. Nat. Geosci. 9.
Grunert, W., Sauerlandt, U., Schlogl, R., Karge, H.G., 1993. XPS investigations of Lanthanum in Faujasite-Type Zeolites. J. Phys. Chem. 97, 1413–1419.
Henderson, P., 1984. General geochemical properties and abundances of the rare earth elements. In: Henderson, P. (Ed.), Rare Earth Element Geochemistry. Elsevier, New York.
Hillier, S., Brydson, R., Delbos, E., Fraser, T., Gray, N., Pendlowski, H., Phillips, I., Robertson, J., Wilson, I., 2016. Correlations among the mineralogical and physical properties of halloysite nanotubes (HNTs). Clay Miner. 51, 325–350.
Huang, G.X., Sun, J.C., Zhang, Y., Chen, Z.Y., Liu, F., 2013. Impact of anthropogenic and natural processes on the evolution of groundwater chemistry in a rapidly urbanized coastal area, South China. Sci. Total Environ. 463, 209–221.
Huang, J., He, H., Tan, W., Liang, X., Ma, L., Wang, Y., Qin, X., Zhu, J., 2021. Groundwater controls REE mineralisation in the regolith of South China. Chem. Geol. 577, 120295.
Jemai, S., Amara, A.B., Ben Brahim, J., Plancon, A., 1999. An X-ray diffraction study of two hydrated kaolinites, characterized by 10 and 8.4 angstrom basal distances, is reported. The study is based on a comparison between the experimental and calculated profiles. J. Appl. Crystallogr. 32, 968–976.
Joseph, J., Jemmis, E.D., 2007. Red-, blue-, or no-shift in hydrogen bonds: a unified explanation. J. Am. Chem. Soc. 129, 4620–4632.
Joussein, 2016. Geology and mineralogy of nanosized tubular halloysite. In: Yuan, P., Thill, A., Bergaya, F. (Eds.), Nanosized Tubular Clay Minerals, 7. Elsevier, pp. 12–48.
Joussein, E., Petit, S., Churchman, J., Theng, B., Righi, D., Delvaux, B., 2005. Halloysite clay minerals - a review. Clay Miner. 40, 383–426.
Joussein, E., Petit, S., Fialips, C.-I., Vieillard, P., Righi, D., 2006. Differences in the dehydration-rehydration behavior of halloysites: New evidence and interpretations. Clay Clay Miner. 54, 473–484.
Kynicky, J., Smith, M.P., Xu, C., 2012. Diversity of rare Earth deposits: the Key example of China. Elements 8, 361–367.
Lanson, B., Beaufort, D., Berger, G., Bauer, A., Cassagnabere, A., Meunier, A., 2002. Authigenic kaolin and illitic minerals during burial diagenesis of sandstones: a review. Clay Miner. 37, 1–22.
Lee, K.X., Valla, J.A., 2017. Investigation of metal-exchanged mesoporous Y zeolites for the adsorptive desulfurization of liquid fuels. Appl. Catal. B-Environ. 201, 359–369.
Li, J.P.H., Zhou, X.H., Pang, Y.Q., Zhu, L., Vovk, E.I., Cong, L.N., van Bavel, A.P., Li, S.G., Yang, Y., 2019a. Understanding of binding energy calibration in XPS of lanthanum oxide by in situ treatment. Phys. Chem. Chem. Phys. 21, 22351–22358.
Li, M.Y.H., Zhou, M.F., 2020. The role of clay minerals in formation of the regolith-hosted heavy rare earth element deposits. Am. Mineral. 105, 92–108.
Li, M.Y.H., Zhao, W.W., Zhou, M.F., 2017. Nature of parent rocks, mineralization styles and ore genesis of regolithhosted REE deposits in South China: an integrated genetic model. J. Asian Earth Sci. 148, 65–95.
Li, M.Y.H., Zhou, M.F., Williams-Jones, A.E., 2019b. The genesis of regolith-hosted heavy rare earth element deposits: insights from the world-class zudong deposit in Jiangxi Province, South China. Econ. Geol. 114, 541–568.
Li, M.Y.H., Zhou, M.F., Williams-Jones, A.E., 2020. Controls on the dynamics of rare earth elements during subtropical hillslope processes and formation of regolith-hosted deposits. Econ. Geol. 115, 1097–1118.
Liu, D., Tian, Q., Yuan, P., Du, P., Zhou, J., Li, Y., Bu, H., Zhou, J., 2019. Facile sample preparation method allowing TEM characterization of the stacking structures and interlayer spaces of clay minerals. Appl. Clay Sci. 171, 1–5.
Liu, J., Zhu, R.L., Xu, T.Y., Xu, Y., Ge, F., Xi, Y.F., Zhu, J.X., He, H.P., 2016. Co-adsorption of phosphate and zinc(II) on the surface of ferrihydrite. Chemosphere 144, 1148–1155.
Lu, Y.Q., Wang, R.C., Lu, X.C., Li, J., Wang, T.T., 2016. Reprint of Genesis of halloysite from the weathering of muscovite: Insights from microscopic observations of a weathered granite in the Gaoling Area, Jingdezhen, China. Appl. Clay Sci. 119, 59–66.
Madejová, J., Gates, W.P., Petit, S., 2017. IR Spectra of Clay Minerals. In: Gates, W.P., Kloprogge, J.T., Madejová, J., Bergaya, F. (Eds.), Infrared and Raman Spectroscopes of Clay Minerals, vol. 8. Elsevier, pp. 107–149.
Moldoveanu, G.A., Papangelakis, V.G., 2012. Recovery of rare earth elements adsorbed on clay minerals: I. Desorption mechanism. Hydrometallurgy 117-118, 71–78.
Nesbitt, H.W., 1979. Mobility and fractionation of rare earth elements during weathering of a granodiorite. Nature 279, 206–210.
Ram, R., Becker, M., Brugger, J., Etschmann, B., Burcher-Jones, C., Howard, D., Kooyman, P.J., Petersen, J., 2019. Characterisation of a rare earth element- and zirconium-bearing ion-adsorption clay deposit in Madagascar. Chem. Geol. 522, 93–107.
Sanematsu, K., Watanabe, Y., 2016. Characteristics and genesis of ion adsorption-type rare earth element deposits. In: Verplanck, P.L., Hitzman, M.W. (Eds.), Rare Earth and Critical Elements in Ore Deposits. Society of Economic Geologists, pp. 55–80.
Sanematsu, K., Moriyama, T., Sotouky, L., Watanabe, Y., 2011. Mobility of rare earth elements in basalt-derived laterite at the Bolaven Plateau, Southern Laos. Resour. Geol. 61, 140–158.
Sanematsu, K., Kon, Y., Imai, A., Watanabe, K., Watanabe, Y., 2013. Geochemical and mineralogical characteristics of ion-adsorption type REE mineralization in Phuket, Thailand. Mineral. Deposita 48, 437–451.
Saxton, K.E., Rawls, W.J., 2006. Soil water characteristic estimates by texture and organic matter for hydrologic solutions. Soil Sci. Soc. Am. J. 70, 1569–1578.
Schoonheydt, R.A., Johnston, C.T., 2013. Surface and interface chemistry of clay minerals. In: Bergaya, F., Lagaly, G. (Eds.), Handbook of Clay Science, vol. 5. Elsevier, pp. 139–172.
Singh, B., 1996. Why does halloysite roll? – a new model. Clay Clay Miner. 44 (2), 191–196.
Slansky, E., 1985. Interstratificaiton of 10-Å and 7-Å layers in halloysite – allegras mixing function for random and partially ordered stacking. Clay Clay Miner. 33, 261–264.
Suga, S., Imada, S., Muro, T., Fukawa, T., Shishidou, T., Tokura, Y., Moritomo, Y., Miyahara, T., 1996. La 4d and Mn core absorption magnetic circular dichroism, XPS and inverse photoemission spectroscopy of La1-xSrxMnO3. J. Electron Spectrosc. Relat. Phenom. 78, 283–286.
Tan, D.Y., Yuan, P., Annabi-Bergaya, F., Liu, D., He, H.P., 2015. Methoxy-modified kaolinite as a novel carrier for high-capacity loading and controlled-release of the herbicide amitrole. Sci. Rep. 5.
Tian, F.P., Wu, W.C., Jiang, Z.X., Liang, C.H., Yang, Y.X., Ying, P.L., Sun, X.P., Cai, T.X., Li, C., 2006. The study of thiophene adsorption onto La(III)-exchanged zeolite NaY by FT-IR spectroscopy. J. Colloid Interface Sci. 301, 395–401.
Tian, J., Chi, R.A., Yin, J.Q., 2010. Leaching process of rare earths from weathered crust elution-deposited rare earth ore. Trans. Nonferrous Metals Soc. China 20 (5), 892–896.
Vieira, C.C., Botelho, N.F., Gamier, J., 2019. Geochemical and mineralogical characteristics of REEY occurrences in the Mocambo Granitic Massif tin-bearing A-type granite, Central Brazil, and its potential for ion-adsorption-type REEY mineralization. Ore Geol. Rev. 105, 467–486.
Viers, J., Oliva, P., Dandurand, J.L., Dupré, B., Gaillardet, J., 2007. Chemical weathering rates, CO2 consumption, and control parameters deduced from the chemical composition of rivers. In: Holland, H.D., Turekian, K.K. (Eds.), Treatise on Geochemistry. Pergamon, pp. 1–25.
Woo, M.K., Huang, L.J., Zhang, S.X., Li, Y., 1997. Rainfall in Guangdong province, South China. Catena 29, 115–129.
Xie, Y., Hou, Z., Goldfarb, R.J., Guo, X., Wang, L., 2016. Rare earth element deposits in China. In: Verplanck, P.L., Hitzman, M.W. (Eds.), Rare Earth and Critical Elements in Ore Deposits. Society of Economic Geologists.
Yang, M., Liang, X., Ma, L., Huang, J., He, H., Zhu, J., 2019. Adsorption of REEs on kaolinite and halloysite: a link to the REE distribution on clays in the weathering crust of granite. Chem. Geol. 525, 210–217.
Yang, S.Q., Yuan, P., He, H.P., Qin, Z.H., Zhou, Q., Zhu, J.X., Liu, D., 2012. Effect of reaction temperature on grafting of gamma-aminopropyl triethoxysilane (APTES) onto kaolinite. Appl. Clay Sci. 62-63, 8–14.
Yaraghi, A., Ariffin, K.S., Baharun, N., 2019. A short review on REE recovery from ion-adsorption clays. Aspects Min. Miner Sci. 2 (15), 342–344.
Yaraghi, A., Ariffin, K.S., Baharun, N., 2020. Comparison of characteristics and geochemical behaviors of REEs in two weathered granitic profiles generated from

metamictized bedrocks in Western Peninsular Malaysia. J. Asian Earth Sci. 199, 104385.
Yariv, S., Shoval, S., 1976. Interaction between Alkli-halides and Halloysite - IR Study of Interaction between Alkali-halides and Hydrated Halloysite. Clay Clay Miner. 24, 253–261.
Yuan, P., 2016. Thermal-treatment-induced deformations and modifications of halloysite. In: Yuan, P., Thill, A., Bergaya, F. (Eds.), Nanosized Tubular Clay Minerals, 7. Elsevier, pp. 12–48.
Yuan, P., Southon, P.D., Liu, Z.W., Green, M.E.R., Hook, J.M., Antill, S.J., Kepert, C.J., 2008. Functionalization of halloysite clay nanotubes by grafting with gamma-aminopropyltriethoxysilane. J. Phys. Chem. C 112, 15742–15751.
Yuan, P., Tan, D.Y., Annabi-Bergaya, F., 2015. Properties and applications of halloysite nanotubes: recent research advances and future prospects. Appl. Clay Sci. 112, 75–93.
Yuan, P., Du, P., Zhou, J., Wang, S., 2019. Insights into the geological and resource significance of aluminosilicate nanominerals. Acta Petrol. Sin. 35, 164–176.
Zhang, R.Q., 2011. Distribution and cycle of water on the earth. In: Zhang, R.Q., Liang, X., Jin, M.G., Wan, L., Yu, Q.C. (Eds.), Fundamentals of Hydrogeology, 6th ed. Geological Publishing House, pp. 9–13.